Sorkio, Anni E.; Vuorimaa-Laukkanen, Elina P.; Hakola, Hanna M.; Liang, Huamin; Ujula, Tiina A.; Valle-Delgado, Juan Jose; Osterberg, Monika; Yliperttula, Marjo L.; Skottman, Heli

Biomimetic collagen I and IV double layer Langmuir-Schaefer films as microenvironment for human pluripotent stem cell derived retinal pigment epithelial cells

Published in:
Biomaterials

DOI:
10.1016/j.biomaterials.2015.02.005

Published: 01/05/2015

Document Version
Peer-reviewed accepted author manuscript, also known as Final accepted manuscript or Post-print

Biomimetic Collagen I and IV double layer Langmuir-Schaeffer films as microenvironment for human pluripotent stem cell derived retinal pigment epithelial cells

Anni Sorkio[1,], Elina Vuorimaa-Laukkanen[2], Hanna Hakola[2], Huamin Liang[2], Tiina Ujula[3], Juan José Valle-Delgado[3], Monika Österberg[3], Marjo Yliperttula[4] and Heli Skottman[1]*

[1]BioMediTech, University of Tampere, Biokatu 12, 33520 Tampere, Finland;

[2]Department of Chemistry and Bioengineering, Tampere University of Technology, Korkeakoulunkatu 8, 33720 Tampere, Finland;

[3]Department of Forest Products Technology, School of Chemical Technology, Aalto University, P.O. Box 16300, 00076 Aalto, Finland;

[4]Division of Biopharmaceutical Sciences, Centre for Drug Research, Faculty of Pharmacy, University of Helsinki, Viikinkaari 5, 00790 Helsinki, Finland;

*Corresponding author, Anni Sorkio, BioMediTech, Biokatu 12, 33520 Tampere, **Finland; Tel.: +358 40 1901790, Fax: fax: +358 33551 8498; E-mail address: anni.sorkio@uta.fi**

Abstract

The environmental cues received by the cells from synthetic substrates *in vitro* are very different from those they receive *in vivo.* In this study, we applied the Langmuir-Schaeffer (LS) deposition, a variant of Langmuir-Blodgett technique, to fabricate a biomimetic microenvironment mimicking the structure and organization of native Bruch's membrane for the production of the functional human embryonic stem cell derived retinal pigment epithelial (hESC-RPE) cells. Surface pressure-area isotherms were measured simultaneously with Brewster angle microscopy to investigate the self-assembly of human collagens type I and IV on air-subphase interface. Furthermore, the structure of the prepared collagen LS films was characterized with scanning electron microscopy, atomic force microscopy, surface plasmon resonance measurements and immunofluorescent staining. The integrity of hESC-RPE on double layer LS films was investigated by measuring transepithelial resistance and permeability of small molecular weight substance. Maturation and functionality of hESC-RPE cells on double layer collagen LS films was further assessed by RPE-specific gene and protein expression, growth factor secretion, and phagocytic activity. Here, we demonstrated that the prepared collagen LS films have layered structure with oriented fibers corresponding to architecture of the uppermost layers of Bruch's membrane and result in increased barrier properties and functionality of hESC-RPE cells as compared to the commonly used dip-coated controls.

Keywords: Biomimetic material, Collagen structure, Langmuir Blodgett film, Retinal pigment epithelial cell, Ophthalmology, Retina, Human embryonic stem cell

1. Introduction

Cells in tissues are influenced by the extracellular matrix (ECM) in which they reside [1,2]. Apart from the mechanical support, ECM binds soluble factors and regulates their distribution and presentation to cells, as well as plays an important role in cell morphology, migration, proliferation, differentiation and maturation [3-5]. While synthetic scaffolds made of biocompatible materials have been shown to closely mimic the ECM structure, they still lack much of the fine, intricate architecture and biochemical cues that can be found in the native ECM [6]. Thus, the environmental cues received by the cells from these substrates *in vitro* are very different from those they receive *in vivo* [7].

Dysfunction and irreversible damage of the retinal pigment epithelium (RPE) layer is a fundamental factor in the progression of degenerative retinal diseases, such as age-related macular degeneration (AMD) [8,9]. Human embryonic stem cells (hESCs) are an attractive cell source for cell transplantation therapies to treat AMD due to their limitless supply [10] and ability to differentiate towards functional RPE cells [11,12]. Cell transplants of hESC–derived RPE (hESC-RPE) cells are currently under clinical trials for the treatment of the dry form of AMD and Stargardt's disease [13] and clinical trials with autologous human induced pluripotent stem cell (hiPSC)-derived RPE cell sheets for the wet type of AMD are starting soon [14].

In vivo, the RPE cells rest on a specific pentalaminar 1-4 µm thick ECM sheet called Bruch's membrane. Bruch's membrane is located between the RPE and the underlying choroid, where it provides structural support for the RPE cells as well as operates as a biological filter to allow for the reciprocal exchange of nutrients, biomolecules and metabolic waste products. Histologically, Bruch's membrane composes of five different layers with distinguishable structure and composition. The basement membrane of RPE forms the outermost layer of the

Bruch's membrane, and it mainly consists of collagen type IV, laminin, fibronectin, hyaluronic acid, heparan sulfate and chondroitin/dermatan sulphate whereas the inner collagenous layer comprises of collagen type I, III, and V [15].

Collagen has been extensively examined as a supportive structure for a variety of tissues such as skin, cartilage, bone, corneal and nerve tissues [16-18]. Human primary RPE cells and the immortalised ARPE-19 cell line have been previously cultured on equine, bovine and rat collagen type I membranes [19-22] as well as on human collagen type I thin films [23]. Furthermore, porcine collagen type I gels have been used for the maturation of hiPSC-RPE cells in studies aiming for clinical applications [14]. In addition, gelatin, which is collagen that has been processed to remove its higher organized structure, has been widely studied with RPE [24-26]. To the best of our knowledge, collagen type IV has been assessed with RPE cells and hESC-RPE cells merely in the form of protein coating [27-29]. Despite the success with collagen in biomedical applications, mimicking the natural fiber orientation and structure remains a major challenge [30-32].

The Langmuir–Blodgett (LB) technique is an attractive approach for obtaining artificial biomimetic models with a well-characterized molecular organization without the use of additives and bio-incompatible materials [30,33,34]. This approach is based on the presence of collagen in its molecular form in acidic solution and its ability to form fibers resulting from the increase of the solvent pH when it is spread onto the subphase surface [35]. In the LB technique, this process is forced to take place at the air-subphase interface in a Langmuir trough. The interface is subsequently compressed to obtain oriented collagen fibers and deposited onto a solid substrate [34]. When the deposition of the floating monolayer from the subphase surface onto a solid support occurs horizontally, the technique is referred to as Langmuir–Schaeffer (LS) deposition

[36]. In previous studies, human fibroblasts, 3T3 mouse fibroblastic cells and adipose-derived stem cells have been shown to respond favorably to the oriented rat and calf collagen I films prepared with LB technique [34,37]. Along with collagen I, laminin, fibronectin and vitronectin thin LB films have been previously manufactured [38].

In this study, we have applied the LS technique to fabricate a biomimetic microenvironment mimicking the structure and organization of native Bruch's membrane for the production of the clinically relevant hESC-RPE cells. A layered and oriented collagen film from human collagen types I and IV was manufactured only based on human origin biomaterials. The constructed film had two separate layers, collagen type I layer underneath and collagen type IV layer above corresponding the inner collagenous layer and the basement membrane of Bruch's membrane, respectively. Here, we demonstrate that the prepared LS films have layered structure with oriented fibers and result in increased barrier properties and functionality of hESC-RPE cells as compared to commonly used dip-coated controls.

2. Experimental methods

2.1.Preparation of collagen solutions

The human collagen I (Col I) and human collagen IV (Col IV) from human placenta (Sigma-Aldrich St. Louis, MO, USA) were treated according to the protocol described by Goffin et al. [34]. Briefly, both collagens were dissolved into dilute acetic acid (Merck, Germany) to obtain a solution of 1 mg ml^{-1} and pH ~ 3. Prior to Langmuir-film preparation, collagen solutions were sonicated in water bath on ice for two 10 minute periods with a 10 minute rest period in between. These solutions were prepared fresh right before use.

2.2. Langmuir isotherms and Brewster Angle Microscopy (BAM)

The full isotherms and Brewster angle microscope (BAM) images were measured simultaneously with a KSV OPTREL BAM300 mounted on a KSV minitrough Langmuir film balance (KSV Instruments) equipped with a double barrier system. Dulbecco's phosphate buffered saline (DPBS) (Lonza Group Ltd., Basel, Switzerland) was used as a subphase: two-fold DPBS solutions were prepared in Milli-Q water. The temperature of the subphase was 20.8 ± 0.5^{o}C and the compression speed for the isotherms and Langmuir-film preparation was 65 mm min^{-1} i.e. 48.75 cm^{2} min^{-1}. 180 µl of the 1 mg ml^{-1} collagen solution was spread drop-wise onto the subphase using a glass microsyringe. The film was allowed to equilibrate for 30 minutes before compression. The BAM instrument was equipped with a 10 mW HeNe laser (633 nm) linearly polarized in the plane of incidence by a Glann-Thomson polarizer. The reflection from the interface passes through a second Glann-Thomson polarizer and was collected by a CCD camera. The microscope was adjusted so that the background reflection from the bare air-water interface was minimal. The spatial resolution of the system was approximately 2 µm.

2.3. Langmuir-Schaeffer (LS) films

The LS films were prepared using the KSV minitrough system. The Langmuir-film was prepared as described above. The film was compressed to the deposition pressure of 12 mN m^{-1} for Col I and 30 mN m^{-1} for Col IV and allowed to stabilize for 15 min before deposition on substrates. The compression of the LS films took place symmetrically and horizontally. Several types of substrates were used for LS-transfer: silicon wafers for scanning electron microscopy (SEM) studies, freshly cleaved mica for atomic force microscopy (AFM) measurements, SPR sensor substrates (ca. 50 nm gold with a chromium adhesion layer of ca. 2 nm coated on glass slides) for SPR, borosilicate glass coverslips (0.13 mm thickness, VWR Collection, VWR, Finland) for immunofluorescence stainings and commercial polyethylene terephthalate (PET)

cell culture inserts with 5 µm pore size (Millipore) for cell culture and permeability studies. Prior to the deposition the glass substrates were cleaned by 10 min sonication in chloroform and chromic sulfuric acid. After careful rinsing with water the glass substrates were kept 30 min in 1 mM NaOH (Merck KGaA, Germany) and subsequently dried in an oven at 120 ^{o}C. The silicon wafers were cleaned by sonicating 1 min in isopropanol and rinsing with chloroform followed by drying in nitrogen flow. Before deposition, the SPR sensor substrates were first cleaned by boiling them in the cleaning solution of NH_4OH (30%) (Merck KGaA): H_2O_2 (30%) (Merck Schuchardt OHG, Germany): Milli-Q H_2O (1:1:5) for 10 min. The LS films were transferred onto substrates manually by touch-and-lift method. Thereafter, the deposited LS films were dried in a desiccator for a minimum of 24 hours to evaporate any remainings of the subphase. Subsequently, the samples were washed twice with Milli-Q H_2O to remove the formed salt crystals and dried again before measurements or the deposition of a second layer. For the double layer Col I and Col IV LS films, Col IV LS film was deposited on top of a dried Col I LS film as described above. The manufacturing process of the LS films is illustrated in Supplementary Fig. 1.

2.4. Dip-coating

For control samples, substrates were dip-coated with collagen protein solutions as described previously [11,27]. Briefly, substrates were rinsed with DPBS, and immersed in collagen protein solution at a concentration of 5 µg cm^{-2} for 3 hours at +37^{o}C. The following substrates were used for dip-coating: freshly cleaved mica for AFM measurements, SPR sensor substrates for SPR, borosilicate glass coverslips for immunofluorescence stainings and commercial PET cell culture inserts with 5 µm pore size for cell culture studies. The pH of collagen solution during coating

procedure was 7. Prior to material characterization and cell seeding, the dip-coated control samples were rinsed twice with DPBS to remove any remaining of unbound protein.

2.5. Scanning electron microscopy (SEM)

The microstructure of the LS films deposited on silicon substrates was observed using field-emission scanning electron microscope (FE-SEM, Carl Zeiss Ultra 55).

2.6. Atomic force microscopy (AFM)

A MultiMode 8 atomic force microscope (Bruker Corporation, Massachusetts, USA) equipped with a J scanner and Nanoscope V controller was used to characterize the nanostructure of different collagen LS films. Images were obtained in air using silicon NSC15/AlBS cantilevers (MicroMasch, Tallinn, Estonia) with a tip radius below 10 nm, operating in tapping mode. Research NanoScope 8.15 software (Bruker Corporation) was utilized for image analysis.

2.7. Surface plasmon resonance (SPR)

Surface plasmon resonance (SPR) measurements were performed with an MP-SPR Navi 200-L instrument equipped with two light source pairs providing 654 and 782 nm, as well as 668 and 783 nm, wavelengths (BioNavis Ltd., Tampere, Finland). Before the deposition of the collagen films, all pre-cleaned MP-SPR sensors were measured in air and water to acquire the backgrounds. Thereafter, the MP-SPR sensor substrates with deposited collagen layers were measured in water and then in air. All SPR measurements were performed at the wavelengths of 654 and 782 nm, and 668 and 783 nm at 20 °C. The original SPR data were processed using the BioNavis Data viewer software. The measured MP-SPR spectra for pure SPR sensors were fitted with a free Fresnel equation based program Winspall 3.02 in order to extract the thickness (d) and refractive index (n). During the fitting, the optical parameters from the pure gold fitting were

used as backgrounds for multilayer modeling. The refractive index was kept constant but the thickness of the layers was fitted. This fitting procedure was repeated for the n-values with an increment of 0.2 between 1.4-1.6. Thus, the d-n continuum solutions were acquired. In order to investigate the stability of deposited collagen LS layers on the gold surface they were monitored in real time with SPR at 782 nm under. The water flow flush was running at 30 µl/min at 20 °C for up to 10 h. The measured SPR sensograms were processed using the BioNavis Data viewer software.

2.8. Human embryonic stem cell derived retinal pigment epithelial cells

In this study, we investigated two hESC lines, Regea 08/023 (46, XY) and Regea 11/013 (46, XY), which were previously derived in our laboratory [39]. The undifferentiated hESCs were maintained on Mitomycin C-treated (Sigma-Aldrich) mitocally inactivated human foreskin fibroblast feeder cells (CRL-2429TM, ATCC, Manassas, VA, USA) in serum-free conditions and enzymatically passaged using TrypLE Select (Invitrogen, UK) onto fresh feeder cells at ten-day intervals. Undifferentiated hESCs were differentiated into RPE cells as described previously [11].

After 55 to 132 days of differentiation in suspension culture, the pigmented areas of the floating aggregates were manually selected and cut with a lancet, dissociated with Trypsin-EDTA (Lonza, Walkersville, MD) and replated to Col IV-coated 24-well culture plates (Corning® CellBIND®, Corning Inc., NY, USA). Thereafter, the pigmented cells were enriched in adherent cultures for 180-209 days. The hESC-RPE maturation and functionality was investigated on Col I-Col IV double layer LS films. The double layer LS films were sterilized under ultra violet light for 10 minutes per each side of the film and hydrated in culture medium for 1 h before cell seeding. For plating cells on LS films, the hESC-RPE cells were dissociated

with TrypLE Select (Invitrogen), filtered through BD Falcon cell strainer (BD Biosciences) and seeded on LS films at density of 1.2×10^5 cells cm^{-2}. Commercial cell culture inserts with 1 µm pore size (Millipore) dip-coated with collagen IV (5 µg cm^{-2}) were selected as control in cell culture studies as we have previously used Col IV for enrichment and maturation of hPSC-RPE cells [11,27].

2.9. Gene expression analysis

After 42 days of culture, the gene expression of RPE-specific proteins bestrophin (*BEST*), microphthalmia-associated transcription factor (*MITF*), pigment epithelium-derived factor (*PEDF*), retinal pigment epithelium specific protein 65 kDa (*RPE65*) and tyrosinase (*TYR*) as well as pluripotency marker octamer-binding transcription factor (*OCT*)3/4was assessed with reverse transcription–polymerase chain reaction (RT-PCR). Glyceraldehyde 3-phosphate dehydrogenase (*GAPDH*) was used as an endogenous control. RNA was extracted using NucleoSpin RNA II kit (Macherey-Nagel, GmbH & Co) according to the manufacturer's instructions. Water was used as a negative control in RT-PCR analysis to detect any impurities in the reagents and procedure. The gene expression of pluripotency markers *OCT3/4* and *Nanog* and RPE-specific proteins *RPE65* and *TYR* were also investigated for undifferentiated hESCs in both investigated cell lines. Detailed RT-PCR protocol and primer sequences have been previously reported [11].

Differences in relative expression level of *RPE65* gene were studied further with quantitative real-time PCR (qPCR) as described previously [27]. Samples were collected from two individual experiments. TaqMan® Gene Expression Assays (Applied Biosystems Inc.) with FAM-labels were used for PCR reaction: *RPE65* (Hs01071462_m1) and *GAPDH* (Hs99999905_m1). The results were analyzed using 7300 System SDS Software (Applied Biosystems Inc.). The relative

quantification of *RPE65* was calculated using the 2-ΔΔCt method [40]. The values for each sample were normalized to expression levels of *GAPDH*. The expression level of dip-coated control was set as the calibrator in both investigated cell lines (fold change equals 1).

2.10. Immunocytochemistry

The fiber-like structure of Col I, Col IV and double layer Collagen LS films as well as the protein expression and localization of hESC-RPE cells on double layer LS films was examined with immunofluorescence (IF) staining. The expression of pluripotency marker OCT3/4 was investigated for the undifferentiated hESCs with IF stainings. Samples were washed twice with DPBS, fixed with 4% paraformaldehyde (Sigma-Aldrich) for 10 min at room temperature (RT), washed with DPBS and permeabilized with 0.1% Triton X-100 in DPBS (Sigma-Aldrich) at RT for 10 min. Next, unspecific binding sites were blocked with 3% BSA (Sigma-Aldrich) at RT for 1 h. Thereafter, samples were incubated with primary antibodies overnight in 4 ^{o}C: rabbit anti-bestrophin 1:400, mouse anti-CRALBP 1:600, mouse anti-Na^{+}/K^{+}ATPase 1:100, rabbit anti-MITF 1:350 (all from Abcam, Cambridge, UK), mouse anti-collagen IV , rabbit anti-collagen I 1:200 (both from Millipore), mouse anti-MERTK 1:50 (Abnova), mouse anti-zonula occludens 1 (ZO-1) 1:250 (Invitrogen) and goat anti-OCT3/4 1:200 (R & D Systems Inc., Minneapolis, MN). Cells were washed several times with DPBS. Secondary antibodies were diluted in ratio of 1:800 with 0.5% BSA-DPBS: Alexa Fluor 568- conjugated goat anti-mouse IgG and goat anti-rabbit Ig G, and Alexa Fluor 488-conjugated donkey anti-rabbit IgG, donkey anti-mouse IgG and donkey anti-goat IgG (all from Molecular Probes, Life Technologies). In addition, Phalloidin-Tetramethylrhodamine B isothiocyanate 1:400 (Sigma-Aldrich) was used for labeling filamentous actin. Samples were incubated in secondary antibody dilutions for 1 h in RT following repeated washes in DPBS. 4',6'diamidino-2-phenylidole (DAPI) included in the

mounting media was used for staining the nuclei (Vector Laboratories Inc., Burlingame, CA). To verify that the fiber-like organized structure of the LS films is due to the organization of collagen to the air-subphase interface and compression of the surface, we carried out immunostainings of Col I- and Col IV-dip-coated samples (coating concentration for both 5 µg cm^{-2}). Images were taken with Olympus BX60 microscope (Olympus, Tokyo, Japan) or LSM 700 confocal microscope (Carl Zeiss, Jena, Germany) using a 63x oil immersion objective. Images were edited using ZEN 2011 Light Edition (Carl Zeiss) and Adobe Photoshop CS4.

2.11. Western blotting

The RPE65 protein expression was studied further after 42 days of culture on double layer LS films with Western blotting as previously described [27]. Mouse anti-RPE65 (1:5000, Millipore) and mouse anti-β-actin (1:5000, Santa Cruz) primary antibodies were used. The RPE65 protein expression was quantified with band area calculation in Image J Image Processing and Analysis Software and compared to the loading control β-actin from the same lane in the membrane. These RPE65/β-actin ratios were calibrated against dip-coated control samples in both investigated cell lines (RPE65/β-actin ratio for controls equals 1) in order to carry out relative comparison between controls and LS films.

2.12. Transepithelial resistance

The integrity and barrier function of the forming hESC-RPE on LS films were studied with transepithelial resistance (TER) measurements after 42 days of culture. Samples were tightly clamped to a P2307 slider (Physiologic Instruments, San Diego, CA), and assembled to a custom-made Teflon chamber as previously described [41]. Measurements were carried out in DPBS with a Millicell electrical resistance system volt-ohm meter (Merck Millipore, Darmstad, Germany). TER-values (Ωcm^2) were calculated by subtracting the value of empty material sheet

without cells from the result, and by multiplying the result by the surface area of the substrate. Calculated TER-values were normalized against the dip-coated controls in both investigated cell lines. TER-values were obtained from three individual experiments with four parallel samples for each condition.

2.13. Permeability study

The ability of LS films to act as semipermeable barrier and the integrity of hESC-RPE monolayer on double layer LS films was assessed by measuring the flux of a small molecular weight (700 Da) Alexa Fluor® 568 Hydrazide sodium salt (Life Technologies) at a concentration of 0.0065 mM. The permeability of hESC-RPE cells on LS films was studied after 64 days of culture. The study was carried out in Ussing chamber system (Physiologic Instruments, San Diego, CA) with P2300 chambers and P2307 sliders and culture medium without KnockOut™ Serum Replacement (KO-SR) was used as a diffusion medium. The chambers were maintained at 37^{o}C by using a circulating water bath and gas inflow was applied to the chambers. The donor chamber was filled with 2.1 ml of diffusion medium with fluorescent marker, whereas equal volume of diffusion medium without fluorescent marker was applied on the receptor chamber. Volumes of 100 µl were sampled from the receptor chamber at 60, 120, 180, 240 and 300 min and replaced with fresh diffusion medium. The fluorescence of the samples was analyzed in 96-well plates using the Wallac Victor2™ 1420 Multilabel counter (Perkin Elmer-Wallace, Norton, OH)) at 590 nm excitation and 642 nm emission wavelengths. The diffusion of Alexa Fluor® 568 Hydrazide sodium salt across the LS films and hESC-RPE monolayers was characterized by calculating the apparent permeability coefficient (P_{app}, cm^2s^{-1}) as $P_{app} = dC/dt/(60C_0A)$, where dC/dt is the slope of the linear portion of the permeability curve, C_0 is the initial concentration in the donor chamber, and A is the exposed surface area of the RPE monolayer (0.031 cm^2).

Furthermore, the data is presented as cumulative permeability illustrating the percentage of diffused fluorescent marker in the receptor chamber compared to initial concentration in the donor chamber over time. Permeability data for hESC-RPE cells on double layer LS films were obtained from three individual experiments with four parallel samples for each condition.

2.14. Phagocytosis

The phagocytic properties of hESC-RPE monolayers on double layer LS films were investigated using isolated porcine photoreceptor outer segments (POS) after 56 days of culture. The POS were isolated as described previously [11]. POS were labeled with fluorescein isothiocyanate (FITC) (0.04 µg/µl; Sigma-Aldrich) in 0.1M $NaHCO_3$ (pH 9) for 1h at RT, following washing three times with PBS and resuspended in culture medium supplemented with 10% fetal bovine serum (FBS, Sigma-Aldrich). HESC-RPE cells on LS films were incubated with POS for 2h at 37^o C. Thereafter, the cells were washed twice with PBS and fixed with 4% paraformaldehyde for 10 min at RT following repeated PBS washings. Subsequently, the cells were permeabilized using 0.1% Triton X-100 for 10 min at RT followed by repeated PBS washings. Filamentous actin was stained with phalloidin (Sigma-Aldrich) by incubating for 30 min at RT following several PBS washings. The nuclei were counterstained with DAPI that was in the mounting media. The images of the hESC-RPE cells with internalized POS fragments were taken using a confocal microscope (LSM 700, Carl Zeiss, 63x oil immersion objective).

2.15. Enzyme-linked immunosorbent assay

The functionality of hESC-RPE cells on LS films was evaluated by their PEDF secretion after 21 days of culture. Culture medium was conditioned with hESC-RPE cells on double layer LS films and dip-coated controls for 24 hours before collecting samples for analysis. PEDF concentration

was determined from the conditioned medium using Chemikine PEDF Sandwich ELISA Kit (Millipore) according to the manufacturer's instructions. Cell density on LS films and controls at day 21 was taken into consideration in PEDF concentration calculations.

Ethical issues:

The National Authority for Medicolegal Affairs Finland has approved our research with human embryos (Dnro 1426/32/300/05). We also have a supportive statement from the local ethics committee of the Pirkanmaa hospital district Finland to derive and expand hESC lines from surplus embryos not used in the treatment of infertility by the donating couples, and to use these cell lines for research purposes (R05116). No new lines were derived for this study.

Statistical analysis

Mann–Whitney U-test and IBM SPSS Statistics software were used for determining statistical significance. Average (median) values of relative TER, P_{app}, and PEDF secretion on LS films were compared to average (median) values obtained on dip-coated controls with Mann–Whitney U-test. P-values ≤ 0.05 were considered statistically significant.

3. Results

3.1. Surface pressure-area isotherms

Isotherms of Col I and Col IV were measured to investigate whether the collagen molecules remain on the DPBS air-subphase interface or enter the subphase instead. During the 30 min stabilization period, the surface pressure increased 0.4 ± 0.2 mN m^{-1} for Col I and 1.4 ± 0.4 mN m^{-1} for Col IV (Fig. 1 (a)). The initial surface pressure after spreading of the collagen solution was 1 mN m^{-1} higher for Col IV compared to Col I although the same amount (in mass) of collagens were used. The pressure versus surface area isotherms for Col I and Col IV are

illustrated in Fig. 1 (b). For Col I the surface pressure did not reach 20 mN m^{-1} before the trough space between the barriers ran out. Instead, the surface pressure of 40 mN m^{-1} was attained for Col IV. Spreading more Col I only led to a shift of the isotherm to higher areas per gram. For both collagens, a steady increase in surface pressure was detected upon compression of the interface between the barriers. For deposition of LS films and for further analysis and cell culture studies, the surface pressures of 12 and 30 mN m^{-1} were used for Col I and Col IV, respectively.

3.2. Fiber formation, orientation and structure of collagen LS films

BAM was used to detect the Col I and Col IV Langmuir film formation and fiber orientation in the DPBS-air interface during compression. Both Col I and Col IV covered the surface evenly and no pure subphase surface was observed after spreading. At low surface pressures the collagen molecules floated loosely on the surface, and neither orientation nor fiber-like structures were observed. As the surface pressure increased, during both stabilization and compression periods, the images got brighter as the density of collagen on the air-subphase interface increased. For Col I, the fiber formation was clearly observed during compression as nearly vertical 10 μm thick and 50 μm long structures were visible already 27 s after the compression was started (Fig. 1 (c)). At this point, the pressure had increased only 1 mN m^{-1} from that measured after the 30 min stabilization period. For Col IV, darker domains with lower collagen density or thickness were observed (Fig. 1 (d)). The domains differed in size from small nearly circular areas with 10 μm diameter to larger 200 μm × 100 μm areas. At 10 – 20 mN m^{-1} the shape of the domains changed from irregular to elongated ellipses which were oriented according to the compression direction. Highly organized structures oriented parallel to the barriers were observed with both collagens (Fig. 1. (c-d)). At all pressures the BAM images of Col IV were brighter than those of Col I.

The microstructure of LS films was assessed with SEM. In the SEM images, a thin film with a fiber-like structure similar to those observed in BAM figures were detected (Fig. 1. (e-f)). The substrates were completely covered by both Col I and Col IV LS films. During deposition of the second layer of the double layer LS film, the angle of the substrate towards compression direction was changed. Thus, the presence of both Col I and Col IV layers can be clearly seen as ordered structures of different angles (Fig. 1. (g)).

The fiber formation and structure was studied further with IF staining. Beautiful oriented fibers were observed with Col I LS films (Fig. 1. (i)) whereas the structure of Col IV LS films appeared more net-like (Fig. 1. (k)). These results are similar to those seen in both BAM and SEM images. The dip-coated controls had neither fiber-like nor organized structure (Fig. 1. (j-l)). The IF images of the double layer LS film confirmed the presence of both Col I and Col IV layers (Fig. 1. (h)). As detected with SEM, the Col I and Col IV films in double layer LS films had organized structure and the layers were oriented at different angles, with Col I LS film deposited underneath the net-like Col IV LS layer.

The barrier properties of LS films were assessed using a small molecular weight (700Da) fluorescent marker. The P_{app} for Col I LS films was $21 \times 10^{-5} \pm 8 \times 10^{-5}$ cm^2 s^{-1} and for Col IV $26 \times 10^{-5} \pm 5 \times 10^{-5}$ cm^2 s^{-1}, whereas a slightly smaller value of $15 \times 10^{-5} \pm 5 \times 10^{-5}$ cm^2 s^{-1} was detected for double layer LS film (Fig. 1. (m)). For empty PET insert P_{app}-value of $17 \times 10^{-5} \pm 2$ x 10^{-5} cm^2 s^{-1} was recorded. The cumulative permeability for Col I and Col IV LS films is shown in Fig. 1. (n) and for double layer LS film and empty PET insert in Fig. 1. (o). Compared to the empty PET insert, Col I LS film did not form a barrier for the small molecular weight marker. Instead, decrease in the cumulative permeability of Col IV LS films was detected. However, after 300 min exposure, this barrier was disturbed. A similar decrease in cumulative permeability

was observed for double layer LS film as detected for Col IV LS film. Instead, no sudden changes and disturbance in barrier property was noticed during 300 min exposure time for the double layer LS film.

3.3. Nanostructure and the stability of the collagen LS films

The nanostructure of the collagen LS films was investigated with AFM (Fig. 2. (a-h)). The width of the collagen fibers was determined from the analysis of the height topographic profiles of AFM images (Fig. 2. (i-l)) Average values of about 4.5 nm and 12.5 nm were obtained for the fibrils of Col I and Col IV LS films, respectively. Widths up to 65 nm and 140 nm were also observed for larger fibers of collagen I and IV, respectively. The Col IV LS films had more of a net-like structure. Interestingly, the surface topography of the double layer LS film was different from the monolayer Col IV LS film even though Col IV LS film was the uppermost layer of both samples.

The deposited LS films were further characterized with two-media (air and water) MP-SPR measurements in order to extract the unique solution of refractive index (d) and thickness (n). [42] Examples of the Winspall fitting in air and water at 782 nm for washed collagen LS films are shown in Fig. 3 (a) and for unwashed films in Supplementary Fig. 2. Good fits and clear angle shifts between the collagen layers and the background were observed both in air and in water. The gathered d and n continuum solutions were then plotted in order to find the intersection of air and water, which is the actual thickness and refractive index (an example illustrated in Fig. 3 (b)). Thicknesses of different collagen LS films measured by MP-SPR are summarized in Fig. 3 (c). The average thickness of the unwashed Col I LS films was less than 11 nm whereas the Col IV LS films showed much higher values reaching up to 31 nm. The thickness of the double layer LS film, 27 nm, was significantly lower than the sum of Col I and

Col IV monolayer LS films. The thickness of Col I LS film reduced during washing procedure down to 7 nm. Instead, for Col IV and double layer LS films the difference between unwashed and washed samples was insignificant. The thickness of the dip-coated collagen IV control was only 5 nm.

The stability of the deposited collagen layers in the water flow was evaluated by monitoring the real-time signal change with MP-SPR. Merely small changes in the angle were observed (Supplementary Fig. 3): the highest angle decrease was 0.08 degrees, which is much less than the angle shifts induced by the deposited layers (between 0.9 – 2.7 degrees, Supplementary Table 1). Furthermore, the SPR signals became constant after about 6000 s. In all cases, the largest shifts were detected for unwashed samples and the highest changes were observed for Col IV LS films.

3.4. Human ESC-RPE growth on collagen LS films

Undifferentiated hESCs in both cell lines grew as colonies with defined borders (Supplementary Fig. 4 (a)), were positive for pluripotency marker OCT3/4 in IF stainings (Supplementary Fig. 4 (b)) and also expressed pluripotency markers *OCT3/4* and *Nanog* on gene expression level. The expression of RPE-specific proteins *RPE65* and *TYR* was negative for the undifferentiated cells (Supplementary Fig. 4 (c)). hESC-RPE cell adhesion and maturation on LS films was evaluated with light microscopy imaging, immunofluorescent staining, gene expression analysis and western blotting after 42 days of culture (Fig. 4). Both investigated hESC-RPE cell lines had formed confluent and uniform RPE monolayer throughout the entire double layer LS films with abundant pigmentation and typical hexagonal RPE cell morphology (Fig. 4 (a-b)). Furthermore, the hESC-RPE cells on LS films formed more uniform and smoother epithelium compared to the dip-coated controls (Supplementary Fig. 5). hESC-RPE cells from both used cell lines showed

expression of Na^+/K^+ATPase on the apical membrane, demonstrating polarization of the formed epithelia (Fig. 4 (c)). Moreover, hESC-RPE cells were positive for mature RPE-related proteins bestrophin, CRALBP, MITF, MERTK and RPE65 (Supplementary Fig. 6) on all investigated substrates.

Gene expression analysis confirmed the expression of mature RPE markers *BEST*, *MITF*, *PEDF*, *RPE65* and *TYR* on double layer LS films as well as on controls (Fig. 4 (d)). Furthermore, there was no expression of the pluripotency marker *OCT3/4* on double layer LS films and on dip-coated controls (Supplementary Fig. 7). However, hESC-RPE cells on double layer LS films showed increased gene expression of *RPE65* compared to the dip-coated control samples in qPCR analysis (Fig. 4 (e)). The *RPE65* expression on LS films increased up to 2.1-fold in Regea 08/023 hESC-RPE cells, whereas 2.4-fold expression was seen with Regea 11/013 hESC-RPE cells. However, the increase in expression level of *RPE65* was significantly higher on LS film only with Regea 08/023 hESC-RPE cells ($p < 0.05$). Similar trend in RPE65 synthesis was also detected in protein expression level with western blot analysis. In both investigated cell lines, hESC-RPE cells on LS films showed higher expression of RPE65 compared to the dip-coated controls (Fig. 4 (f-g)); 3.6- and 1.3-fold expression levels were confirmed for Regea 08/023 and Regea 11/013 hESC-RPE cells on double layer LS films, respectively.

3.5.Barrier properties of hESC-RPE cells on layered collagen LS films

The barrier properties of hESC-RPE cells on double layer LS films were examined with IF staining, TER measurements and permeability studies. hESC-RPE cells on LS films showed uniform expression of tight junction protein ZO-1, while more discontinuous and heterogeneous labeling against ZO-1 was detected on the dip-coated controls (Fig. 5 (a-b)). The integrity of

hESC-RPE epithelia on double layer LS films was investigated further with TER-measurements following 42 days of culture. In both studied hESC-lines, the TER-values were significantly higher ($P < 0.005$) on LS films compared to hESC-RPE cells grown on dip-coated controls (Fig. 5 (c)). With Regea 08/023 hESC-RPE cells, measured TER-values reached 2.4 ± 0.6 –fold on LS films compared to the controls. Similar increase in TER-values was seen with Regea 11/013 hESC-RPE cells with 2.0 ± 0.4-fold higher relative TER on LS films.

Junctional integrity of hESC-RPE cells was assessed by measuring the flux of 700 Da fluorescent markers at the concentration of 0.0065 mM (Fig. 5 (d-f)). In both investigated cell lines, the hESC-RPE on double layer LS films resulted in significantly lower permeability ($p < 0.05$) compared to dip-coated controls, with P_{app}-values of $1.76 \times 10^{-6} \pm 5.78 \times 10^{-7}$ cm^2 $s^{-1}$and $2.48 \times 10^{-6} \pm 1.99 \times 10^{-6}$ cm^2 $s^{-1}$for Regea 08/023 and Regea 11/013 hESC-RPE cells, respectively (Fig. 5 (d)). P_{app}-values for dip-coated control samples reached for $3.86 \times 10^{-6} \pm 2.49 \times 10^{-6}$ cm^2 s^{-1} for Regea 08/023 hESC-RPE cells and $4.93 \times 10^{-6} \pm 2.09 \times 10^{-6}$ cm^2 s^{-1} for Regea 11/013 hESC-RPE cells. After 5 hour exposure time, the cumulative permeability for 700 Da molecules on double layer LS films was 0.10 ± 0.03 % for Regea 08/023 hESC-RPE cells and 0.13 ± 0.06% for Regea 11/013 hESC-RPE cells, whereas 0.23 ± 0.04 % and 0.28 ± 0.07 % were measured for Regea 08/023 and 11/013 hESC-RPE cells on dip-coated controls (Fig. 5 (e-f)).

3.6. Functionality of hESC-RPE cells on double layer collagen LS films

The functionality of hESC-RPE cells on double layer LS films was assessed with *in vitro* phagocytosis assay after 56 days of culture. Internalized POS were seen in both investigated cell lines on double layer LS films as well as on dip-coated controls, confirming that the hESC-RPE cells on studied collagen films possess phagocytic activity (Fig. 6(a-d)). However, major

differences were found in PEDF secretion of hESC-RPE cells on double layer LS films compared to the dip-coated controls. hESC-RPE cells on LS films showed highly significant ($p < 0.005$) increase in PEDF secretion with both studied cell lines after 21 days of culture (Fig. 6 (e)). PEDF secretion was 1682 ± 167 ng ml^{-1} for Regea 08/023 hESC-RPE cells and 853 ± 146 ng ml^{-1} for Regea 11/013 hESC-RPE cells on LS films, whereas lower PEDF concentrations of 274 ± 118 ng ml^{-1} and 207 ± 155 ng ml^{-1} were measured for Regea 08/023 hESC-RPE cells and Regea 11/013 hESC-RPE cells on controls, respectively.

4. Discussion

The microenvironments where the cells reside in tissues affect the characteristics of cells including cell morphology, polarity and function [43]. Microenvironment of the cells *in vivo* is a combination of multiple complex factors. The surrounding extracellular matrix and the structural environment of the cells is one of them [44]. However, the classic cell culture substrates do not provide the natural environment for the cultured cells *in vitro*, potentially effecting on the clinical outcome of cells in tissue engineering applications [7,43]. Furthermore, it is difficult to generate a substrate that possesses similar properties to the tissue environment and that can be produced in a reproducible manner [45]. In this study, we manufactured a biomimetic microenvironment mimicking the layered structure and composition of the Bruch's membrane from human sourced collagens I and IV for the production of the functional hESC-RPE cells. To our awareness, the present study is the first to demonstrate the preparation of oriented and fiber-like collagen type IV LS films as well as culture of hESC-RPE cells on thin layer by layer deposited double layer collagen films with oriented fiber-like structure.

Collagen molecules precipitate out of solution and form fibers at neutral pH [35]. Here, we demonstrated a steady increase in surface pressure upon compression of the interface

between the Langmuir trough barriers for both Col I and Col IV LS films. This steady increase in surface pressure during compression indicates that both collagens resided at the air-subphase interface. These results are in good agreement with those previously reported for Col I LB films [30,34,46]. With both collagens, a clear increase in surface pressure was detected after the spreading of the collagens initially dissolved in acidic solution onto the neutral subphase. This increase in surface pressure during stabilization period could be caused by the potassium and phosphate ions in the DPBS subphase, both of which have been shown to affect the fiber formation and structure of the forming collagen fibrils [47]. Based on our observations, this self-assembly of collagens on the air-subphase interface was not an instant process. However, equilibrium was reached after 30 min stabilization period. The higher surface pressure of Col IV after the stabilization period as well as the brighter images seen with BAM during compression indicates that more Col IV remains at the air-subphase interface than that of Col I.

BAM analysis confirmed the formation of oriented structures during compression. Previously, the collagen type I fibers have been shown to orient parallel to the Langmuir trough barriers [34]. This is in accordance with our findings with Col I as well as with Col IV LS films. In contrast to LS films, no fiber-like oriented networks were detected with Col I and Col IV dip-coated controls in IF stainings, implying that the fiber-like organization of the collagen networks is due to the application of the collagen solution on the air-subphase interface and subsequent compression [33]. The presence of the Col I and Col IV LS films in double layer LS structures was confirmed with SEM and IF analysis, in which the two oriented collagen layers could be distinguished by the different angle between the oriented fiber layers. This is in line with previously reported results for layered collagen type I LB films [30].

High resolution AFM images allowed detailed analysis of the assembly of collagen molecules into fibrillar structures. The inner collagenous layer of Bruch's membrane consists of 60 nm thick striated fibres of collagen I, III and V [15]. In the present study, the average thickness for the fiber-like structures detected with AFM for Col I LS films was 4.5 nm, suggesting that the prepared film consists mainly from tropocollagen triple-helix structures with collagen I microfibrils [32]. The larger microfibril structures detected with AFM had the diameter of 65 nm, indicating that the manufactured Col I LS films had similar fiber-like structures compared to the native inner collagenous layer of Bruch's membrane. The collagen I diameter reported here is closer to its native equivalent compared to a previous study mimicking the inner collagenous layer of human Bruch's membrane, where electrospun collagen I fibers with diameters ranging from 200 to 500 nm were gained [22]. By comparison, the suprastructure of Col IV LS film resulted in a net-like structure formed by smaller 12.5 nm and larger 140 nm thick fibrils, resembling the sheet-like networks of collagen type IV found in basement membranes [48].

One important function of Bruch's membrane is allowing the reciprocal flow of small molecular substances through its layered structure [15]. Collagen type I LB films have been previously reported to be nonporous and free of holes [30]. In contrast in the present study, both individual collagen LS layers as well as the double layer LS film were permeable for small molecular weight fluorescent marker. Interestingly, the barrier function was mainly formed by the Col IV LS layer, but the presence of Col I LS layer was clearly required in the double layer LS film to make the structure mechanically durable enough.

In theory, the thickness of the layered LS film should be equal to the sum of the thickness of the washed Col I and Col IV LS films, i.e. 38-39 nm. However, the measured thicknesses of

the layered LS films in this study were almost 10 nm lower. Similar result has been established previously in a study for layered collagen I LB films, where the mean thickness of monolayer Col I LB films was 20 nm, whereas ten-layer were reported to be 100 nm thick [30]. Likewise, the thicknesses of the washed Col I LS films were decreased compared to the unwashed films. This reduction in expected thickness could be due to a lower binding affinity of the subsequent layers onto the preceding collagen layer governed by differences between the collagen-collagen interactions and those between collagen and the substrate [33,49]. Furthermore, loss of collagen during washing steps between the layer depositions as well as desorption of the salt crystals of the subphase during washing procedure could have also reduced the film thickness. In addition to the change in expected thickness, differences were also seen in the surface topography of the Col IV in the double layer LS film compared to the Col IV monolayer LS film. This indicates that the layer by layer deposited collagens influence the order of them, while deposited as Col I and IV, as is the case in the natural Bruch's membrane. Thus, our study confirms that the first layer affects the structure of the next layer, which is a well known phenomenon in the field of LB films [50].

The arrangement and orientation of ECM dictate cell size, spreading and cell morphology [51]. LS technique enables low-cost and simple method to produce controlled and oriented substrates for tissue engineering applications [30,34]. In the present study, we hypothesized that the double layer LS films would be superior in supporting the hESC-RPE maturation and functionality compared to the conventional dip-coated protein coating. The hESC-RPE cells on LS films displayed RPE specific cobblestone morphology, pigmentation, expression of genes, correct localization of RPE specific proteins, high degree of polarity, as well as phagocytic activity. Importantly, the hESC-RPE cells showed more homogenous epithelium on double layer

LS films compared to the dip-coated controls. Moreover, hESC-RPE cells on LS films demonstrated increased expression of RPE specific protein RPE65 on both gene and protein level in comparison to the dip-coated controls, indicating that the double layer LS films provide more optimal cues for hESC-RPE cell maturation. Previous investigations have found that collagen nanofibers show improved degree of maturation for neural cells against collagen protein coating [52]. Furthermore, Warnke et al. reported that human primary RPE cells cultured on nanofibrous bovine collagen type I membranes resemble the native human RPE [22]. Surprisingly, even though fibroblasts have been shown to align parallel to the Col I LB films [34,37], such orientation was not detected with hESC-RPE cells on double layer LS films. This data suggests that while Col IV LS films showed oriented structure seen in BAM, the netlike supramolecular organization of the Col IV LS films observed with AFM mimic the native organization of the basement membrane and promotes the formation of homogenous epithelium.

The principal function of RPE is to form a dynamic barrier between the neural retina and the choroid [53]. Previously, it has been shown that the ECM protein coating affects the barrier properties of the forming hPSC-RPE epithelium [27]. The hESC-RPE cells on double layer LS films showed significantly increased TER-values as well as clear reduction in the permeability of small molecular weight particles, indicating that the double layer LS films provide a more favorable microenvironment for the development of the barrier properties of the hESC-RPE cells compared to the dip-coated controls. Moreover, a significant increase in PEDF secretion, another important hallmark of the RPE functionality [54,55], was measured for hESC-RPE cells cultured on LS films against dip-coated controls. In a previous study, NB1-RGN cells grown on collagen-blended LB membranes showed increased interferon-β production [38]. In this study, a difference in the functionality of hESC-RPE cells on double layer LS films was detected between

the two investigated cell lines. Previously, it has been shown that individual hESC-lines behave slightly differently, which affects for instance to the appearance of pigmentation during RPE differentiation [56]. Despite the higher PEDF secretion in Regea 08/023 hESC-RPE, hESC-RPE cells derived from both cell lines were significantly more functional on the double layer LS films compared to the dip-coated controls. Hence, the results reported here demonstrate that double layer collagen LS films offer a more natural and appropriate environment for the production of mature and functional hESC-RPE cells.

5. Conclusions

In this study, we demonstrated a LS fabrication technique for generating a biomimetic microenvironment mimicking the structure and organization of native Bruch's membrane from human derived collagens without the use of bioincompatible substances. The prepared thin films showed layered structure with oriented fibers resembling the architecture of the inner collagenous layer and basement membrane of the Bruch's membrane. This study is the first to show successful preparation of organized collagen IV films with fiber-like networks using LS technique as well as the first study to successfully mimic the organized structure and composition of the two uppermost layers of the Bruch's membrane. Furthermore, the prepared double layer collagen LS films were superior in supporting the hESC-RPE maturation and functionality compared to the dip-coated collagen control. Hence, this study demonstrates that the prepared double layer collagen LS films provide a biomimetic microenvironment for the efficient production of hESC-RPE cells *in vitro* potentially increasing their functionality in tissue engineering applications.

Acknowledgements

The authors wish to thank the Academy of Finland (grant numbers 218050, 272808 and 140357), the Finnish Cultural Foundation, Pirkanmaa Regional fund (grant number 50121465) and the Otto A. Malm Foundation. The funders had no role in study design, data collection and analysis, decision to publish, or preparation of the manuscript. Outi Melin, Hanna Pekkanen and Outi Heikkilä are thanked for technical assistance.

References

1. Heino J. The collagen family members as cell adhesion proteins. Bioessays 2007;29:1001-1010.

2. Leitinger B, Hohenester E. Mammalian collagen receptors. Matrix Biol 2007;26:146-155.

3. Hynes RO. The extracellular matrix: not just pretty fibrils. Science 2009;326:1216-1219.

4. Labat-Robert J. Cell-Matrix interactions, the role of fibronectin and integrins. A survey. Pathol Biol (Paris) 2012;60:15-19.

5. Kim DH, Provenzano PP, Smith CL, Levchenko A. Matrix nanotopography as a regulator of cell function. J Cell Biol 2012;197:351-360.

6. Shapira A, Kim DH, Dvir T. Advanced micro- and nanofabrication technologies for tissue engineering. Biofabrication 2014;6:020301-5082/6/2/020301. Epub 2014 May 30.

7. McCarthy JB, Vachhani B, Iida J. Cell adhesion to collagenous matrices. Biopolymers 1996;40:371-381.

8. Gehrs KM, Anderson DH, Johnson LV, Hageman GS. Age-related macular degeneration--emerging pathogenetic and therapeutic concepts. Ann Med 2006;38:450-471.

9. Ambati J, Fowler BJ. Mechanisms of age-related macular degeneration. Neuron 2012;75:26-39.

10. Vazin T, Freed WJ. Human embryonic stem cells: derivation, culture, and differentiation: a review. Restor Neurol Neurosci 2010;28:589-603.

11. Vaajasaari H, Ilmarinen T, Juuti-Uusitalo K, Rajala K, Onnela N, Narkilahti S, et al. Toward the defined and xeno-free differentiation of functional human pluripotent stem cell-derived retinal pigment epithelial cells. Mol Vis 2011;17:558-575.

12. Idelson M, Alper R, Obolensky A, Ben-Shushan E, Hemo I, Yachimovich-Cohen N, et al. Directed differentiation of human embryonic stem cells into functional retinal pigment epithelium cells. Cell Stem Cell 2009;5:396-408.

13. Schwartz SD, Hubschman JP, Heilwell G, Franco-Cardenas V, Pan CK, Ostrick RM, et al. Embryonic stem cell trials for macular degeneration: a preliminary report. Lancet 2012;379:713-720.

14. Kamao H, Mandai M, Okamoto S, Sakai N, Suga A, Sugita S, et al. Characterization of human induced pluripotent stem cell-derived retinal pigment epithelium cell sheets aiming for clinical application. Stem Cell Reports 2014;2:205-218.

15. Booij JC, Baas DC, Beisekeeva J, Gorgels TG, Bergen AA. The dynamic nature of Bruch's membrane. Prog Retin Eye Res 2010;29:1-18.

16. Mollers S, Heschel I, Damink LH, Schugner F, Deumens R, Muller B, et al. Cytocompatibility of a novel, longitudinally microstructured collagen scaffold intended for nerve tissue repair. Tissue Eng Part A 2009;15:461-472.

17. Wang HY, Wei RH, Zhao SZ. Evaluation of corneal cell growth on tissue engineering materials as artificial cornea scaffolds. Int J Ophthalmol 2013;6:873-878.

18. Chajra H, Rousseau CF, Cortial D, Ronziere MC, Herbage D, Mallein-Gerin F, et al. Collagen-based biomaterials and cartilage engineering. Application to osteochondral defects. Biomed Mater Eng 2008;18:S33-45.

19. Thumann G, Hueber A, Dinslage S, Schaefer F, Yasukawa T, Kirchhof B, et al. Characteristics of iris and retinal pigment epithelial cells cultured on collagen type I membranes. Curr Eye Res 2006;31:241-249.

20. Thumann G, Viethen A, Gaebler A, Walter P, Kaempf S, Johnen S, et al. The in vitro and in vivo behaviour of retinal pigment epithelial cells cultured on ultrathin collagen membranes. Biomaterials 2009;30:287-294.

21. Bhatt NS, Newsome DA, Fenech T, Hessburg TP, Diamond JG, Miceli MV, et al. Experimental transplantation of human retinal pigment epithelial cells on collagen substrates. Am J Ophthalmol 1994;117:214-221.

22. Warnke PH, Alamein M, Skabo S, Stephens S, Bourke R, Heiner P, et al. Primordium of an artificial Bruch's membrane made of nanofibers for engineering of retinal pigment epithelium cell monolayers. Acta Biomater 2013;9:9414-9422.

23. Lu JT, Lee CJ, Bent SF, Fishman HA, Sabelman EE. Thin collagen film scaffolds for retinal epithelial cell culture. Biomaterials 2007;28:1486-1494.

24. Lai JY. The role of bloom index of gelatin on the interaction with retinal pigment epithelial cells. Int J Mol Sci 2009;10:3442-3456.

25. Del Priore LV, Tezel TH, Kaplan HJ. Survival of allogeneic porcine retinal pigment epithelial sheets after subretinal transplantation. Invest Ophthalmol Vis Sci 2004;45:985-992.

26. Ho TC, Del Priore LV, Kaplan HJ. En bloc transfer of extracellular matrix in vitro. Curr Eye Res 1996;15:991-997.

27. Sorkio A, Hongisto H, Kaarniranta K, Uusitalo H, Juuti-Uusitalo K, Skottman H. Structure and barrier properties of human embryonic stem cell derived retinal pigment epithelial cells are affected by extracellular matrix protein coating. Tissue Eng Part A 2013.

28. Subrizi A, Hiidenmaa H, Ilmarinen T, Nymark S, Dubruel P, Uusitalo H, et al. Generation of hESC-derived retinal pigment epithelium on biopolymer coated polyimide membranes. Biomaterials 2012;33:8047-8054.

29. Rowland TJ, Blaschke AJ, Buchholz DE, Hikita ST, Johnson LV, Clegg DO. Differentiation of human pluripotent stem cells to retinal pigmented epithelium in defined conditions using purified extracellular matrix proteins. J Tissue Eng Regen Med 2012.

30. Tenboll A, Darvish B, Hou W, Duwez AS, Dixon SJ, Goldberg HA, et al. Controlled deposition of highly oriented type I collagen mimicking in vivo collagen structures. Langmuir 2010;26:12165-12172.

31. Hynes SR, Lavik EB. A tissue-engineered approach towards retinal repair: scaffolds for cell transplantation to the subretinal space. Graefes Arch Clin Exp Ophthalmol 2010;248:763-778.

32. Friess W. Collagen--biomaterial for drug delivery. Eur J Pharm Biopharm 1998;45:113-136.

33. Chen Q, Xu S, Li R, Liang X, Liu H. Network structure of collagen layers absorbed on LB film. J Colloid Interface Sci 2007;316:1-9.

34. Goffin AJ, Rajadas J, Fuller GG. Interfacial flow processing of collagen. Langmuir 2010;26:3514-3521.

35. Jiang F, Horber H, Howard J, Muller DJ. Assembly of collagen into microribbons: effects of pH and electrolytes. J Struct Biol 2004;148:268-278.

36. Langmuir I. Overturning and Anchoring of Monolayers. Science 1938;87:493-500.

37. Pastorino L, Dellacasa E, Scaglione S, Giulianelli M, Sbrana F, Vassalli M, et al. Oriented collagen nanocoatings for tissue engineering. Colloids Surf B Biointerfaces 2014;114:372-378.

38. Higuchi A, Takanashi Y, Ohno T, Asakura T, Cho CS, Akaike T, et al. Production of interferon-beta by fibroblast cells on membranes prepared by extracellular matrix proteins. Cytotechnology 2002;39:131-137.

39. Skottman H. Derivation and characterization of three new human embryonic stem cell lines in Finland. In Vitro Cell Dev Biol Anim 2010;46:206-209.

40. Livak KJ, Schmittgen TD. Analysis of relative gene expression data using real-time quantitative PCR and the 2(-Delta Delta C(T)) Method. Methods 2001;25:402-408.

41. Juuti-Uusitalo K, Delporte C, Gregoire F, Perret J, Huhtala H, Savolainen V, et al. Aquaporin expression and function in human pluripotent stem cell-derived retinal pigmented epithelial cells. Invest Ophthalmol Vis Sci 2013;54:3510-3519.

42. Liang H, Miranto H, Granqvist N, Sadowski JW, Viitala T, Wang B, et al. Surface plasmon resonance instrument as a refractometer for liquids and ultrathin films. Sensors Actuators B: Chem 2010;149:212-220.

43. Alamdari OG, Seyedjafari E, Soleimani M, Ghaemi N. Micropatterning of ECM Proteins on Glass Substrates to Regulate Cell Attachment and Proliferation. Avicenna J Med Biotechnol 2013;5:234-240.

44. Barthes J, Ozcelik H, Hindie M, Ndreu-Halili A, Hasan A, Vrana NE. Cell microenvironment engineering and monitoring for tissue engineering and regenerative medicine: the recent advances. Biomed Res Int 2014;2014:921905.

45. Poole K, Khairy K, Friedrichs J, Franz C, Cisneros DA, Howard J, et al. Molecular-scale topographic cues induce the orientation and directional movement of fibroblasts on two-dimensional collagen surfaces. J Mol Biol 2005;349:380-386.

46. Usha R, Dhathathreyan A, Mandal AB, Ramasami T. Behavior of collagen films in presence of structure modifiers at solid liquid interface. Journal of Polymer Science Part B: Polymer Physics 2004;42:3859-3865.

47. Cooper A. Thermodynamic studies of the assembly in vitro of native collagen fibrils. Biochem J 1970;118:355-365.

48. Kalluri R. Basement membranes: structure, assembly and role in tumour angiogenesis. Nat Rev Cancer 2003;3:422-433.

49. Narayanan B, Gilmer GH, Tao J, De Yoreo JJ, Ciobanu CV. Self-assembly of collagen on flat surfaces: the interplay of collagen-collagen and collagen-substrate interactions. Langmuir 2014;30:1343-1350.

50. Lotta TI, Laakkonen LJ, Virtanen JA, Kinnunen PK. Characterization of Langmuir-Blodgett films of 1,2-dipalmitoyl-sn-glycero-3-phosphatidylcholine and 1-palmitoyl-2-[10-(pyren-1-yl)decanoyl]-sn-glycero-3-phosphat idylcholine by FTIR-ATR. Chem Phys Lipids 1988;46:1-12.

51. Li N, Tourovskaia A, Folch A. Biology on a chip: microfabrication for studying the behavior of cultured cells. Crit Rev Biomed Eng 2003;31:423-488.

52. Yin Y, Huang P, Han Z, Wei G, Zhou C, Wen J, et al. Collagen Nanofibers Facilitated Presynaptic Maturation in Differentiated Neurons from Spinal-Cord-Derived Neural Stem Cells through MAPK/ERK1/2-Synapsin I Signaling Pathway. Biomacromolecules 2014.

53. Rizzolo LJ. Barrier properties of cultured retinal pigment epithelium. Exp Eye Res 2014.

54. Strauss O. The retinal pigment epithelium in visual function. Physiol Rev 2005;85:845-881.

55. Steele FR, Chader GJ, Johnson LV, Tombran-Tink J. Pigment epithelium-derived factor: neurotrophic activity and identification as a member of the serine protease inhibitor gene family. Proc Natl Acad Sci U S A 1993;90:1526-1530.

56. Toivonen S, Ojala M, Hyysalo A, Ilmarinen T, Rajala K, Pekkanen-Mattila M, et al. Comparative analysis of targeted differentiation of human induced pluripotent stem cells (hiPSCs) and human embryonic stem cells reveals variability associated with incomplete transgene silencing in retrovirally derived hiPSC lines. Stem Cells Transl Med 2013;2:83-93.

Figures and Figure captions

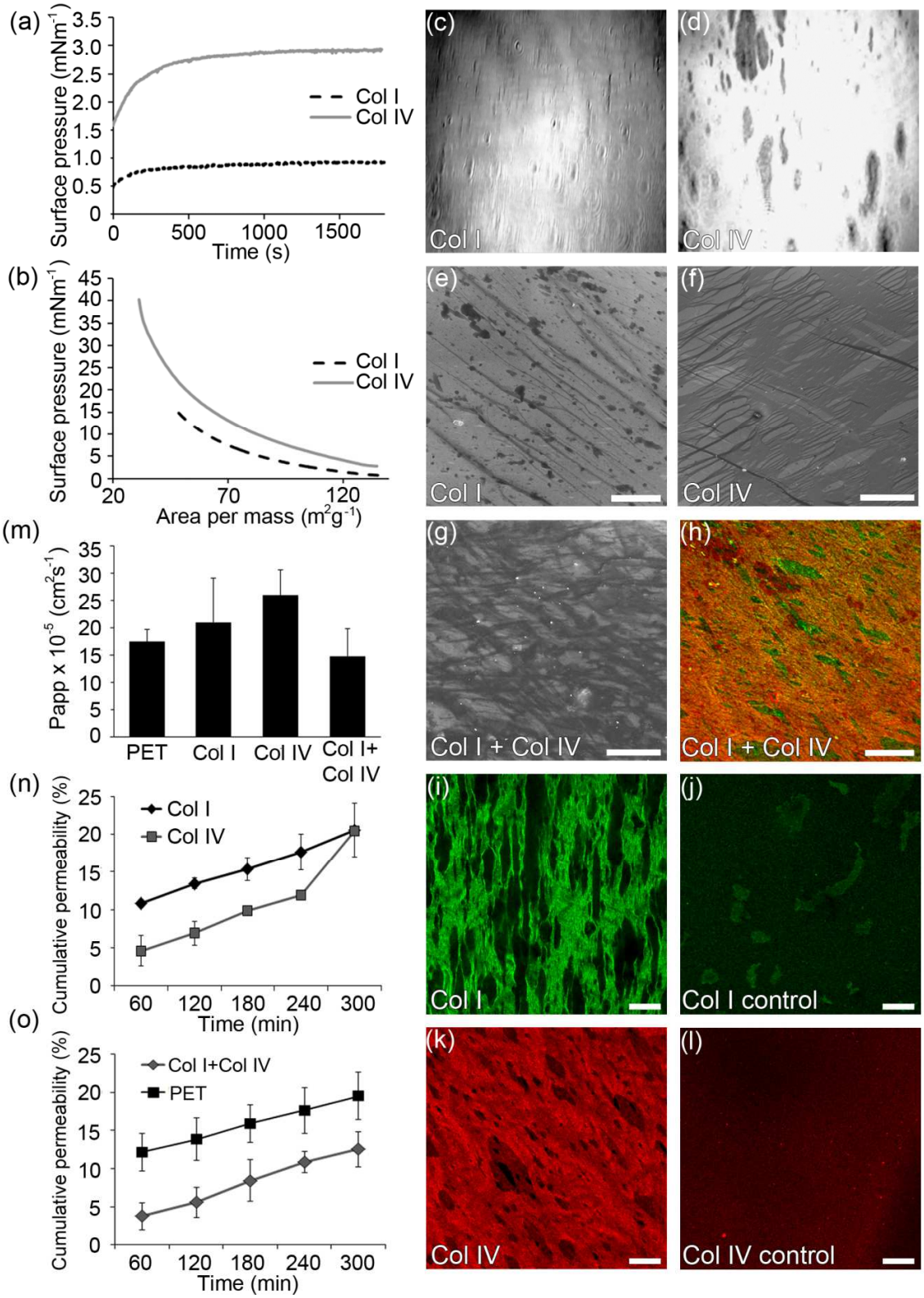

Fig. 1. Fiber formation, orientation and structure of collagen LS films. a) Surface pressure during stabilization after spreading of collagen on subphase and b) surface pressure-area isotherms for Col I and Col IV. BAM images demonstrating the fiber formation during compression of c) Col I and d) Col IV LS films. SEM images of e) Col I, f) Col IV and g) double layer LS films show the microstructure and orientation of prepared LS films. Scale bars e) 40µm and f-g) 20 µm. Immunofluorescence images of h) double layer LS film, i) Col I LS films, j) Col I dip-coated control, k) Col IV LS film and l) Col IV dip-coated control. Collagen I (green) and collagen IV (red). Scale bars h) 20µm and i-l) 50 µm. (m) The apparent permeability coefficient P_{app} and the cumulative permeability of small molecular weight fluorescent marker for n) Col I and Col IV LS films and o) for double layer LS film.

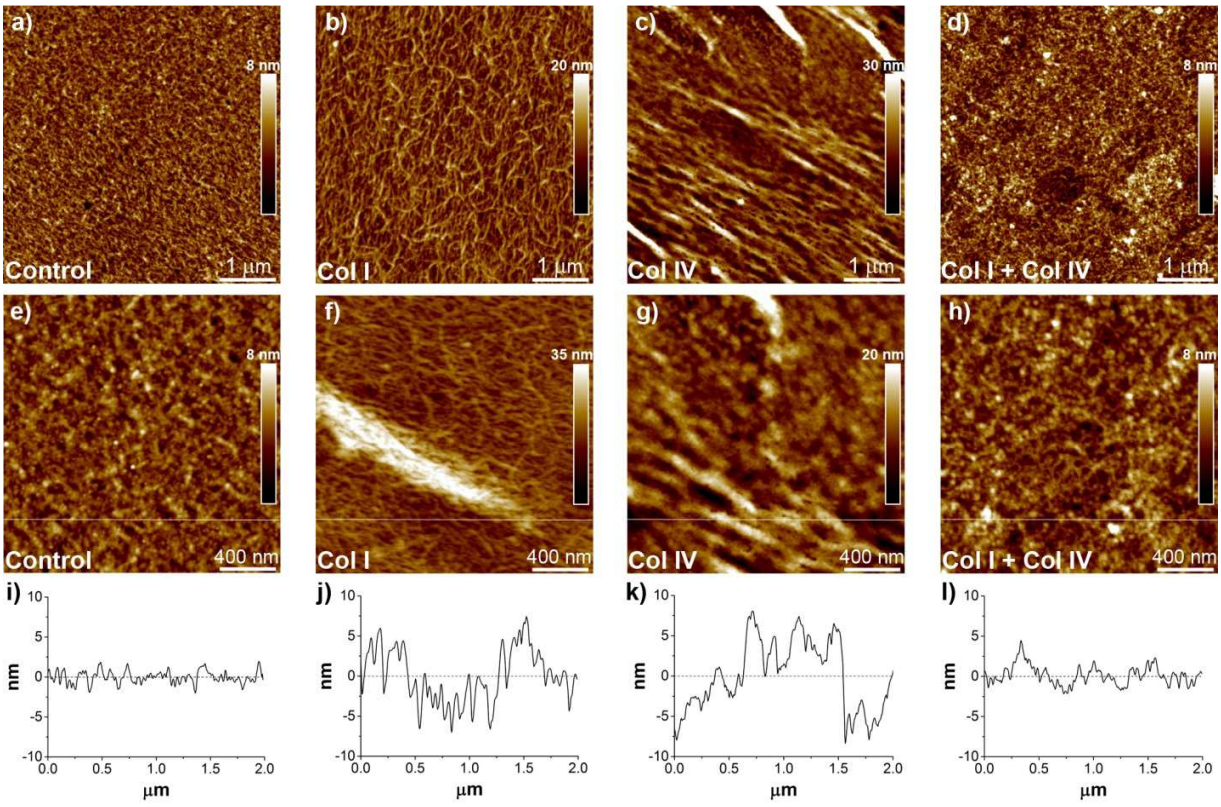

Fig. 2. AFM height images illustrating the nanostructures of different collagen films: a,e) control sample; b,f) Col I LS film; c,g) Col IV LS film; d,h) double layer collagen LS film. i-l) Show the height topographic profiles corresponding to the lines marked in panels e-h), respectively.

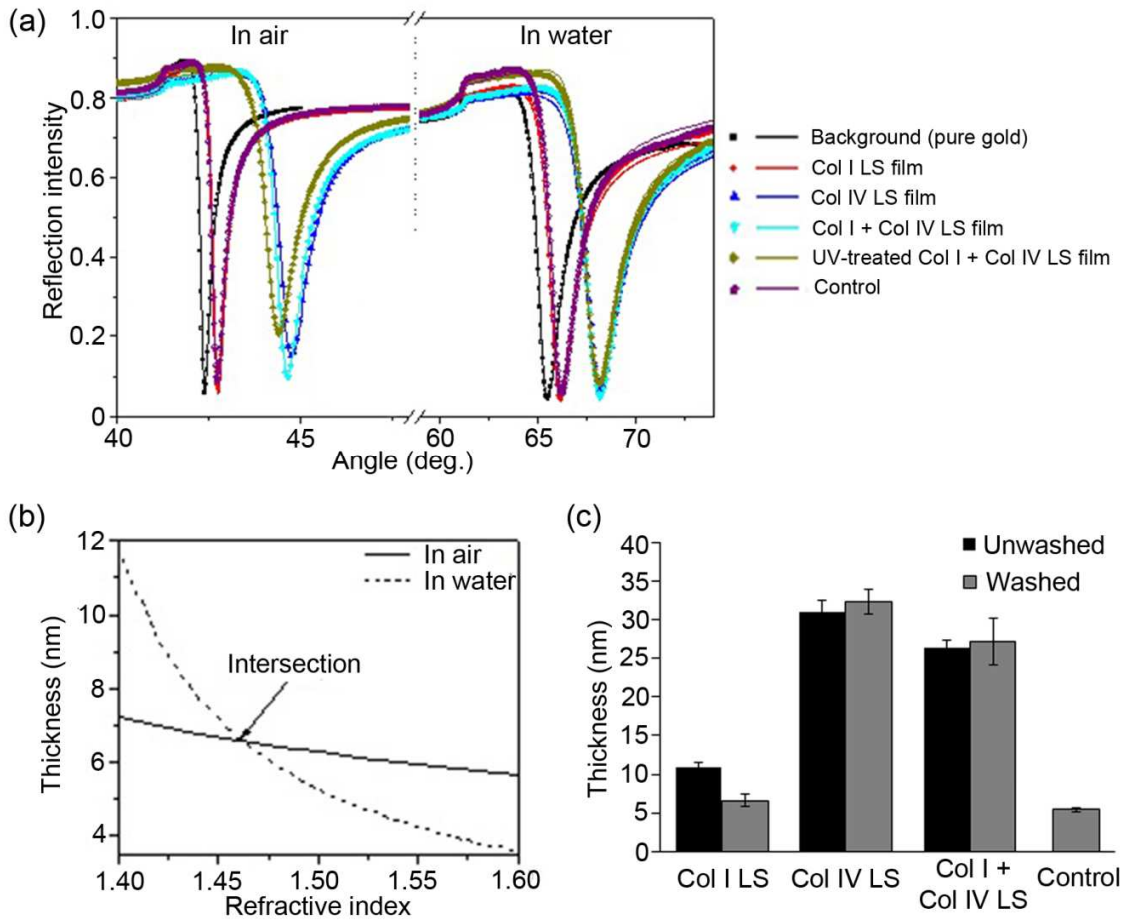

Fig. 3. SPR analysis of LS films. a) Measured MP-SPR angle scans (dots) and the fits (lines) in air and water phase (at 782 nm) of the pure MP-SPR sensor background and the washed deposited collagen LS films on the MP-SPR sensor surfaces. b) Example of the intersection points from the thickness (d) versus refractive index (n) plots for unwashed Col I LS film. c) Thicknesses of deposited collagen layers determined from the two-media (air and water) MP-SPR measurements. The error bars are the standard deviations (SD) from the thicknesses at four different wavelengths.

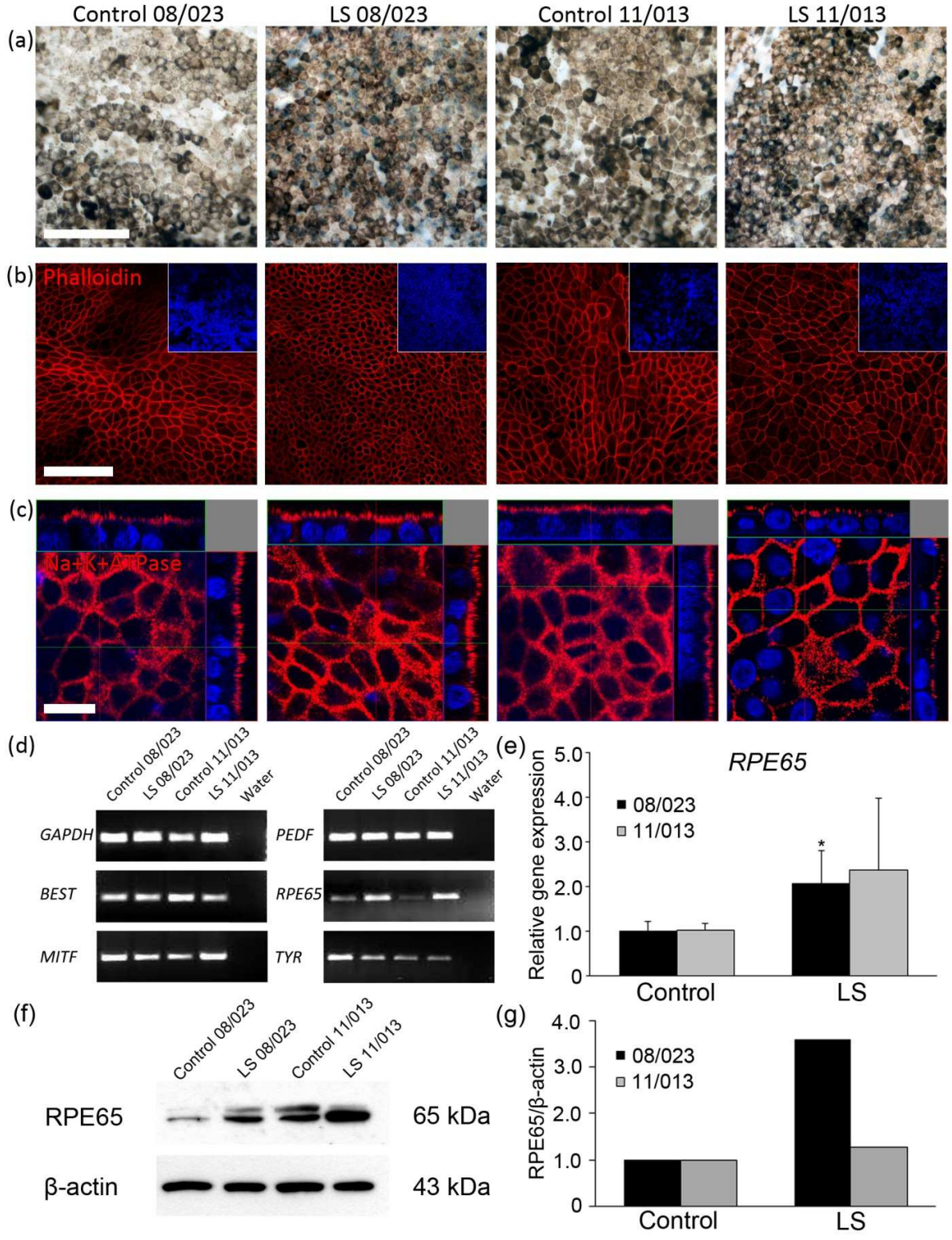
Control 08/023
LS 08/023
Control 11/013
LS 11/013
(a)
(b)
Phalloidin
(c)
Na+K+ATPase
(d)
Control 08/023
LS 08/023
Control 11/013
LS 11/013
Water
GAPDH
BEST
MITF
PEDF
RPE65
TYR
(e)
RPE65
08/023
11/013
Relative gene expression
5.0
4.0
3.0
2.0
1.0
0
*
Control
LS
(f)
RPE65
β-actin
65 kDa
43 kDa
(g)
RPE65/β-actin

Fig. 4. Human ESC-RPE growth on collagen LS films after 42 days of culture. (a) Bright field images illustrating the degree of pigmentation of hESC-RPE cells on double layer collagen LS films. Immunofluorescent staining of (b) phalloidin (red) showing cell morphology and uniformity of the epithelium on collagen films and (c) Na^+K^+ATPase (red) confirming correct polarization of the epithelial monolayers with both investigated cell lines. The nuclei were counterstained with DAPI (blue). (d) Gene expression of mature RPE markers *BEST*, *MITF*, *PEDF*, *RPE65* and *TYR* on LS films. (e) Relative quantitative real-time polymerase chain reaction (qPCR) analysis of *RPE65*. (f-g) Western blot analysis of RPE65 protein expression of hESC-RPE cells on collagen double layer LS films. *=P<0.05 compared to the dip-coated sample. Scale bars (a) and (b) 100 µm and (c) 20 µm.

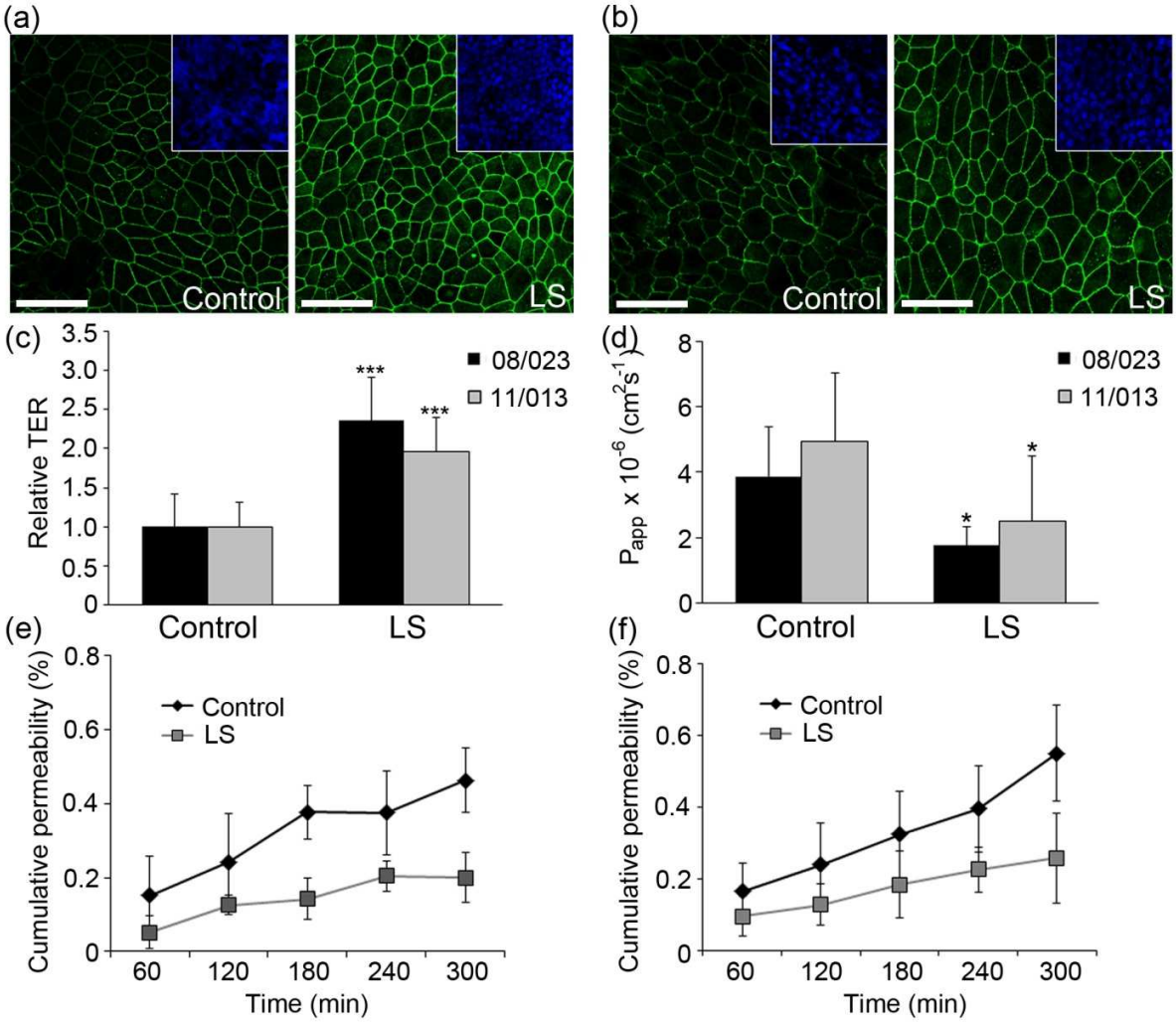

Fig. 5. Barrier properties of hESC-RPE cells on double layer collagen LS film. Expression of tight junction protein zonula occludens 1 (ZO-1) (green) in (a) Regea 08/023 hESC-RPE cells and (b) Regea 11/013 hESC-RPE cells.

The nuclei were counterstained with DAPI (blue). Scale bars 50 µm. (c) Relative transepithelial resistance (TER) of hESC-RPE cells on LS films after 42 days of culture. The apparent permeability coefficient P_{app} (d) and the cumulative permeability of small molecular weight fluorescent marker for (e) Regea 08/023 hESC-RPE cells and (f) Regea 11/013 hESC-RPE cells after 64 days of culture. (d) *=P<0.05 and ***=P<0.005 compared to the control sample.

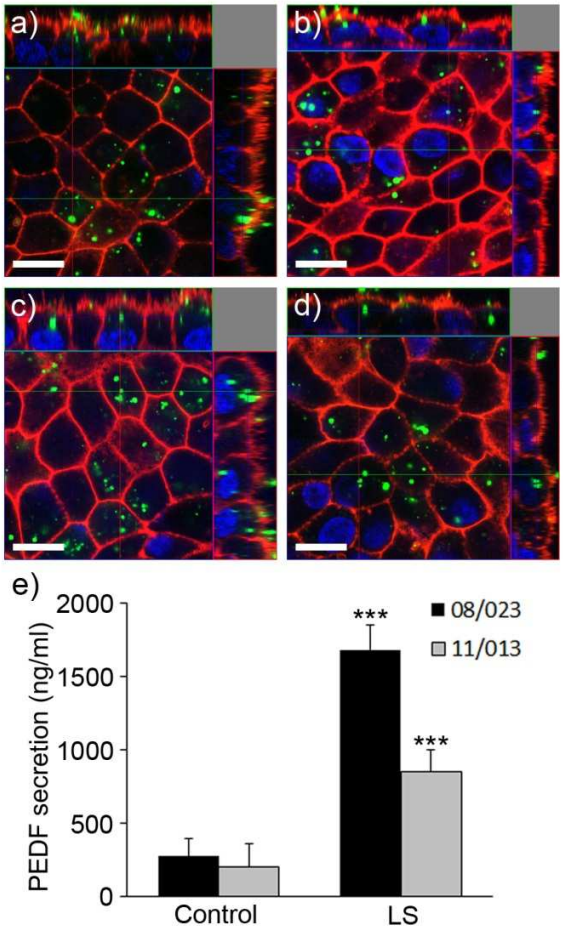

Fig. 6. Functionality of hESC-RPE cells on double layer collagen LS films. The phagocytosis of photoreceptor outer segments (POS) after 56 days of culture (a-d): Regea 08/023 hESC-RPE cells on (a) control and (b) LS film. Regea 11/013 hESC-RPE cells on (c) control and (d) LS films. Filament actin was visualized with phalloidin (red), and the nuclei were counterstained with DAPI (blue). Vertical confocal sections show internalization of POS (green) by hESC-RPE cells on LS films after 2 h culture with porcine POS. Scale bars 10 µm. (e) PEDF secretion of Regea 08/023 and Regea 11/013 hESC-RPE cells on layered LS films after 21 days of culture. ***=P<0.005 compared to the dip-coated control sample.